Epoxide reduction with hydrazine on graphene: A first principles study

Min Chan Kim,[1,a)] Gyeong S. Hwang,[2,b)] and Rodney S. Ruoff[3]
[1]*Department of Chemical Engineering, Cheju National University, Cheju 690-756, Republic of Korea*
[2]*Department of Chemical Engineering, University of Texas, Austin, Texas 78713, USA*
[3]*Department of Mechanical Engineering, University of Texas, Austin, Texas 78713, USA*

(Received 27 February 2009; accepted 15 July 2009; published online 12 August 2009)

Mechanisms for epoxide reduction with hydrazine on a single-layer graphene sheet are examined using quantum mechanical calculations within the framework of gradient-corrected spin-polarized density-functional theory. We find that the reduction reaction is mainly governed by epoxide ring opening which is initiated by H transfer from hydrazine or its derivatives. In addition, our calculations suggest that the epoxide reduction by hydrazine may predominantly follow a direct Eley–Rideal mechanism rather than a Langmuir–Hinshelwood mechanism. We also discuss the generation of various hydrazine derivatives during the reduction of graphene oxide with hydrazine and their potential contribution to lowering the barrier height of epoxide ring opening. © *2009 American Institute of Physics*. [DOI: 10.1063/1.3197007]

I. INTRODUCTION

Since its discovery a few years ago, there has been much excitement about graphene-based materials. Graphene refers to a flat monolayer of carbon atoms packed into a two-dimensional (2D) honeycomb lattice. The 2D crystalline structure opens up a new class of materials with novel electronic, optical, and mechanical properties.[1–7] While offering great promise for many exciting new applications, graphene-based technology currently suffers from the lack of method for high-yield production of graphene. One promising approach that is currently being explored extensively is chemical reduction of exfoliated graphene oxide (GO) sheets with various reducing agents.[8–11]

The basal plane carbon atoms of GO are decorated with hydroxyls and peroxides. The oxygen functionalities make GO sheets hydrophilic, thereby stabilizing them to be easily exfoliated in aqueous media. The exfoliated GO can be chemically reduced to obtain graphene as individual sheets. An effective reduction method is that of placing a graphite oxide paper into a solution of pure hydrazine.[11] The hydrazine reduction in GO results in significant restoration of sp^2 carbon sites but is still unable to completely remove all the oxygen functionalities and often leaves a number of defects.[8–11] Despite its importance, only a very limited effort[10] has been undertaken to understand the mechanism of the hydrazine reduction reaction. In this paper, we present viable pathways for removal of an isolated epoxide group from the graphene surface with hydrazine species based on spin-polarized density-functional theory (DFT) calculations.

II. COMPUTATIONAL METHODS

All atomic structures and energies reported herein were calculated within the GGA (PW91) (Ref. 12) to spin-polarized DFT using the well-established Vienna *ab initio* simulation package (VASP).[13] A plane-wave basis set for valence electron states and Vanderbilt ultrasoft pseudopotentials for core-electron interactions were employed. A plane-wave cutoff energy of 300 eV was used for *ab initio* molecular dynamics (AIMD) simulations and 400 eV for static structure energy calculations. The Brillouin zone integration was performed using a $(4\times4\times1)$ Monkhorst–Pack (MP) mesh of k points for static calculations and a $(2\times2\times1)$ MP mesh for AIMD simulations. In the calculations, periodic boundary conditions with a 32-atom model graphene sheet were employed in all three directions with a vacuum gap of 12 Å in the z direction to separate two distinct surfaces. We used the generalized gradient approximation (GGA)-optimized lattice constant, $a=2.467$ Å, which is slightly larger than the experimental value, 2.461 Å. All atoms were relaxed using the conjugate gradient method until residual forces on constituent atoms became smaller than 1×10^{-2} eV/Å. We carefully checked the convergence of atomic configurations and relative energies with respect to plane-wave energy cutoff, supercell size, and k-point mesh size, confirming that the relative energy variations are in the order of 0.1 eV with unnoticeable changes in the atomic structure. Indeed, the chosen parameters have been found to yield well-converged results for the structure and chemistry of graphite materials.[14–17] We used the nudged elastic band method with 16 intermediate images to determine reaction pathways and barriers, together with the dimer method for the sake of confirmation when necessary.

III. RESULTS AND DISCUSSION

A. O and OH adsorption structure

Earlier theoretical studies[14–17] showed that the site above the middle of a C–C bond is most favorable for atomic oxygen adsorption on the basal plane of graphite, resulting in an epoxidelike structure [left panels in Fig. 1(a)]. Our DFT GGA calculation gives the O binding energy of E_b(O)

[a)]On sabbatical leave in the chemical engineering department at UT-Austin.
[b)]Author to whom correspondence should be addressed. Electronic mail: gshwang@che.utexas.edu. Tel.: 512-471-4847. FAX: 512-471-7060.

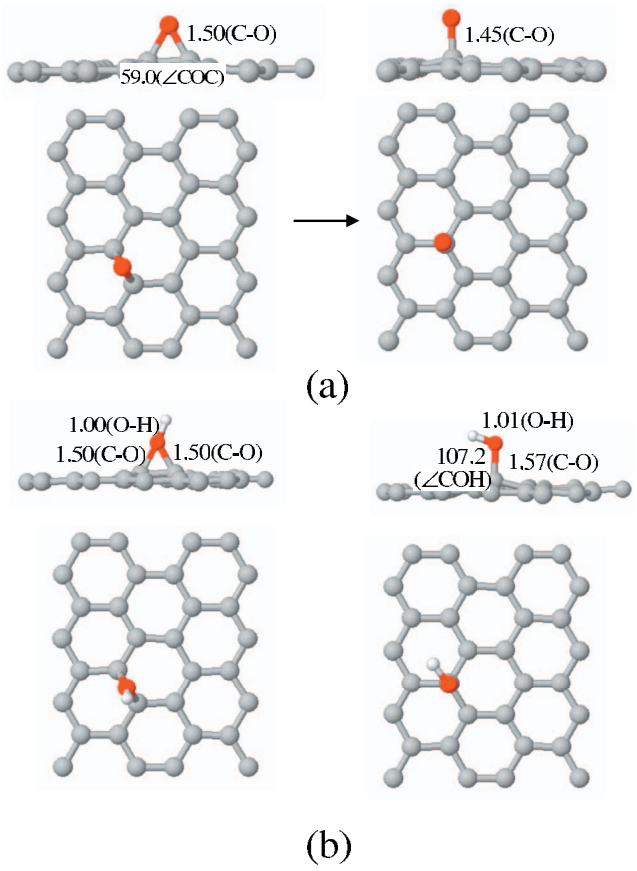

FIG. 1. Top and side views of the optimized adsorption structures of (a) atomic oxygen and (b) hydroxyl radical at the C–C bridge site (left) and the C atop site (right). The gray (gray), red (black), and white (white) balls represent C, O, and H atoms, respectively. Selected bond lengths (in angstroms) and bond angles (in degree) are also indicated.

=62 kcal/mol, in good agreement with previous DFT calculations.[14–17] Here, the binding energy $[E_b(\mathrm{O})]$ is given as

$$E_b(\mathrm{O}) = -E_{\mathrm{O/graphite}} + E_{\mathrm{graphite}} + 1/2E_{\mathrm{O_2}},$$

where $E_{\mathrm{O/graphene}}$, E_{graphene}, and $E_{\mathrm{O_2}}$ represent the total energies of graphene with an epoxide group, graphene, and gas-phase O_2 in the triplet state, respectively. The O–C–C bond angles and C–O and C–C bond lengths of the equilateral triangle structure are estimated to be 60.3°, 1.50 Å, and 1.48 Å, respectively.

As shown in Fig. 1(a) (right panels), we also considered O adsorption on top of a C atom, but the on-top structure easily converts to the epoxide structure with an exothermicity of 13.4 kcal/mol. On the other hand, as illustrated in Fig. 1(b) an OH radical favors the on-top site (directly above a C atom) (right panels) on the defect-free graphene surface, while the C–C bridge site is very unfavorable for OH adsorption (left panels). The predicted OH binding energy at the top site is 15.4 kcal/mol $(=-E_{\mathrm{OH/graphite}}+E_{\mathrm{graphite}}+E_{\mathrm{OH}}$ where E_{OH} refers to the total energy of gas-phase OH), close to other DFT-GGA values.[16] The result demonstrates that hydrogenation of the epoxide O atom will lead to opening of the epoxy ring.

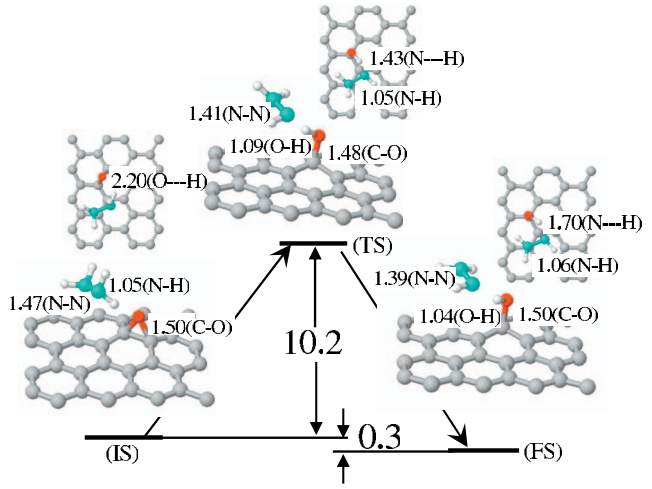

FIG. 2. Optimized configurations for the initial (IS), transition (TS), and final (FS) states of epoxide ring opening via H abstraction from hydrazine (N_2H_4) together with corresponding activation energy and exothermicity (in kcal/mol). For each state, both top and side views are presented. The gray (gray), red (black), cyan (gray in hydrazine), and white (white) balls represent C, O, N, and H atoms, respectively. The bond lengths indicated are given in angstroms [hydrogen bonds are indicated by a dashed line (---)].

B. Epoxide reduction by N_2H_4

A N_2H_4 molecule consists of two pyramidal H_2N subunits which are free to rotate with respect to each other about the N–N single bond. The preferred configuration of N_2H_4 is *gauche* where the electron lone pairs remain approximately perpendicular. Our DFT calculations show that the N_2H_4 molecule can be bound to an epoxide due to electrostatic attraction between a positively charged H in N_2H_4 and the negatively charged O in epoxide. The predicted energy gain is about 4.5 kcal/mol, which is greater than 1.9 kcal/mol estimated for the typical N–H–O hydrogen bond energy. The binding strength of N_2H_4 to the O/graphene surface is not substantial but greater than the average thermal energy at room temperature (≈0.6 kcal/mol).

Figure 2 shows a pathway for epoxide ring opening via H abstraction from N_2H_4, together with an energy variation along the reaction coordinate. The ring-opening reaction is predicted to be nearly thermoneutral while requiring overcoming a barrier of 10.2 kcal/mol which is lower than 13.4 kcal/mol in the absence of N_2H_4 [Fig. 1(a)]. As illustrated in Fig. 1(b), the resulting OH group favorably resides atop a C atom. The results evidently demonstrate that the ring opening of epoxides can be facilitated by hydrazine treatment.

After the first H abstraction, as shown in Fig. 3, the $NHNH_2$ moiety tends to stay around the OH group bound to the graphene surface (indicated as HO-gr hereafter) due to the electrostatic interaction between the positively charged H (in HO-gr) and the negatively charged N (in $NHNH_2$) and/or

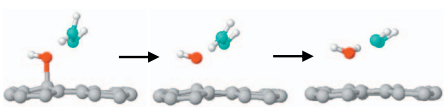

FIG. 3. Snapshots from AIMD for OH hydrogenation via H abstraction from $NHNH_2$. The gray (gray), red (black), cyan (gray, in $NHNH_2$), and white (white) balls represent C, O, N, and H atoms, respectively.

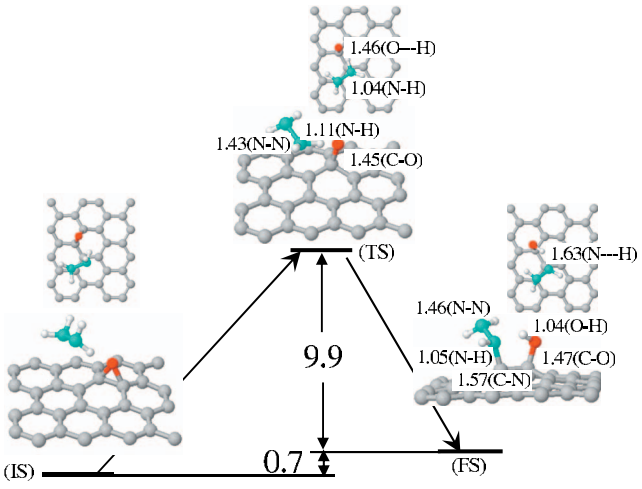

FIG. 4. Optimized configurations for the initial (IS), transition (TS), and final (FS) states of epoxide ring opening via H abstraction from N_2H_4 while leading to coadsorption of OH and $NHNH_2$ at two adjacent sites. The corresponding activation energy and exothermicity (in kcal/mol) are also indicated. For each state, both top and side views are presented. The gray (gray), red (black), cyan (gray), and white (white) balls represent C, O, N, and H atoms, respectively. The bond lengths indicated are given in angstroms [hydrogen bonds are indicated by a dashed line (---)].

between the negatively charged O (in HO-gr) and a positively charged H (in $NHNH_2$). To further look at the reaction between gr-OH and $NHNH_2$, we performed AIMD simulations in the canonical ensemble at various temperatures (ranging from 200 to 300 K) within the Born–Oppenheimer framework. The simulation results show that a H in $NHNH_2$ attacks the O in HO-gr, which in turn weakens the HO-gr interaction [Fig. 3 (left)]. As a result, the OH radical desorbs off the graphene surface while abstracting an additional H atom from the $NHNH_2$ moiety [Fig. 3 (middle)], yielding H_2O and N_2H_2 [Fig. 3 (right)]. The predicted exothermicity of the second H abstraction reaction is 37.2 kcal/mol. At 250 K, the OH hydrogenation occurs in less than 1 ps, implying that the corresponding reaction barrier would be insignificant. Additional AIMD simulations with varying temperatures and initial $NHNH_2$ locations also confirmed the easiness of OH hydrogenation. It is worth emphasizing that all three H atoms in $NHNH_2$ can react with the OH radical, thereby yielding HN=NH or $N-NH_2$ along with H_2O, according to our AIMD simulations. In addition, we find that $NHNH_2$ can escape without the second H abstraction, suggesting possible creation of various hydrazine derivatives (such as $NHNH_2$, NHNH, and NNH_2) during epoxide reduction with hydrazine.

Besides the direct Eley–Rideal (ER) process, we also examined another possible mechanism that involves anchoring of $NHNH_2$ at an on-top site adjacent to HO-gr, after the first H abstraction from gas-phase N_2H_4 (see Fig. 4). The corresponding barrier is predicted to be 10.6 kcal/mol, close to 10.2 kcal/mol for the direct ER case (as shown in Fig. 2). The resulting anchored configuration [Fig. 4 (FS)] appears energetically comparable to the flying configuration [Fig. 2 (FS)], albeit slightly (~1 kcal/mol) unfavorable. The barrier for the interconversion between the final anchored [Fig. 4 (FS)] and flying [Fig. 2 (FS)] configurations is estimated to be 6.2 kcal/mol. In the anchored state, our AIMD shows that the OH and $NHNH_2$ species undergo significant thermal motion due primarily to alternation of three pairwise electrostatic interactions such as $O-H^{+\delta}---N^{-\delta}-HNH_2$, $H-O^{-\delta}---H^{+\delta}-NNH_2$, and $H-O^{-\delta}---H^{+\delta}-NHNH$. However, unlike the flying case, no additional H abstraction from the anchored $NHNH_2$ occurs within a few picoseconds of AIMD simulation time at 500 K.

As presented in Fig. 5, we therefore used a transition search method to calculate the OH hydrogenation reaction, i.e., $HO\text{-}gr+NH_2NH\text{-}gr \rightarrow H_2O(g)+NH2N\text{-}gr$. The reaction is predicted to occur by crossing a barrier of 6.7 kcal/mol with an exothermicity of 23.0 kcal/mol, while the remaining N_2H_2 molecule subsequently desorbs with practically no barrier. Note that the OH hydrogenation barrier is comparable to 6.2 kcal/mol for $NHNH_2$ desorption from the graphene surface. If so, considering entropy effects the $NHNH_2$ desorption can be kinetically more facile than the OH hydrogenation. Indeed, a series of AIMD simulations at 500 K with varying initial HO-gr and NH_2NH-gr configurations demonstrates the occurrence of $NHNH_2$ desorption (while $NHNH_2$ interacts electrostatically with HO-gr) but not OH hydrogenation. Upon desorption, NH_2NH easily donates a H atom to HO-gr, leading to H_2O and N_2H_2 formation as also seen earlier in the direct ER process. The results suggest that the hydrazine reduction of epoxides may predominantly follow the direct ER mechanism rather than the Langmuir–Hinshelwood (LH) mechanism.

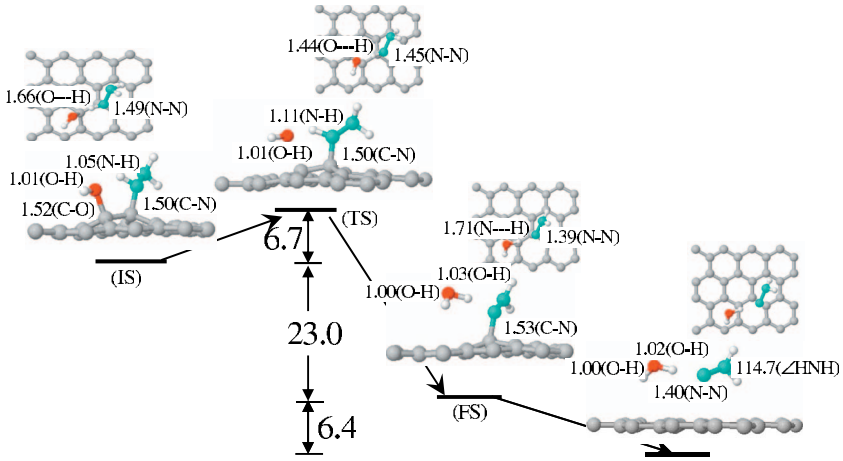

FIG. 5. Optimized configurations for the initial (IS), transition (TS), and final (FS) states of OH hydrogenation via H abstraction from adsorbed $NHNH_2$, leading to the formation of H_2O and N_2H_2. The corresponding activation energy and exothermicities (in kcal/mol) are also indicated. The N_2H_2 is predicted to desorb off the graphene surface with practically no barrier while yielding an exothermicity of 6.4 kcal/mol. For each state, both top and side views are presented. The gray (gray), red (black), cyan (gray), and white (white) balls represent C, O, N, and H atoms, respectively. Selected bond lengths (in angstroms) and bond angles (in degrees) are also indicated [hydrogen bonds are indicated by a dashed line (---)].

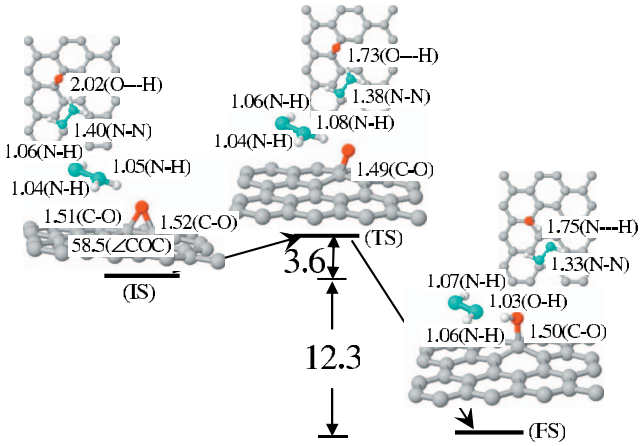

FIG. 6. Optimized configurations for the initial (IS), transition (TS), and final (FS) states of epoxide ring opening via H abstraction from $NHNH_2$, together with the corresponding activation energy and exothermicity (in kcal/mol). For each state, both top and side views are presented. The gray (gray), red (black), cyan (gray), and white (white) balls represent C, O, N, and H atoms, respectively. Selected bond lengths (in angstroms) and bond angles (in degrees) are also indicated [hydrogen bonds are indicated by a dashed line (---)].

Finally, we looked at the possibility that hydrazine derivatives such as $NHNH_2$ will contribute to the epoxide reduction. Figure 6 shows a viable pathway that we identified for epoxy ring opening with $NHNH_2$, together with an energy variation along the reaction coordinate. The predicted barrier height of 3.6 kcal/mol is noticeably lower than 10.2 kcal/mol as estimated for the N_2H_4 case. In addition, the ring-opening reaction with $NHNH_2$ is predicted to be exothermic by 12.3 kcal/mol, whereas the exothermicity of the N_2H_4 case is only 0.3 kcal/mol (albeit practically thermoneutral, see Fig. 2). The relatively facile H abstraction is not surprising considering that $NHNH_2$ is far less stable than N_2H_4 in nature. As illustrated in Fig. 7, we also calculated the reduction of HO-gr with N_2H_4, which turns out to have a small barrier (≈3.5 kcal/mol). Our calculations demonstrate that epoxide reduction in graphene is mainly determined by ring opening that is facilitated by the presence of hydrazine and its derivatives as a source of hydrogen.

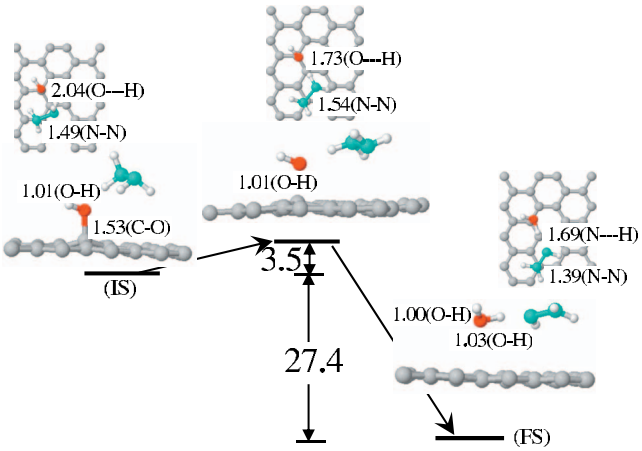

FIG. 7. Optimized configurations for the initial (IS), transition (TS), and final (FS) states of OH hydrogenation via H abstraction from N_2H_4. The reaction is predicted to occur with a small barrier (≈3.5 kcal/mol) while releasing a large exothermicity (≈27.4 kcal/mol). For each state, both top and side views are presented. The gray (gray), red (black), cyan (gray), and white (white) balls represent C, O, N, and H atoms, respectively. The bond lengths indicated are given in angstroms [hydrogen bonds are indicated by a dashed line (---)].

IV. SUMMARY

Atomistic mechanisms for epoxide reduction with hydrazine on graphene are presented based on gradient-corrected spin-polarized DFT calculations. For this study, an epoxide group is placed on a graphene sheet which is modeled using a 32-atom periodic supercell. Our calculations clearly demonstrate that the epoxide is reduced to form H_2O by two successive hydrogenation reactions which involve H abstraction from hydrazine and/or its derivatives. We examined two possible mechanisms, direct ER and LH. We find that both mechanisms are possible with comparable activation barriers (of about 6 kcal/mol), but the ER route is likely to be more kinetically facile. Our study also suggests possible creation of reactive hydrazine derivatives such as $NHNH_2$ during reduction of GO sheets by hydrazine, while they can contribute to facilitating epoxide reduction. Here we should admit that the reaction of hydrazine species with epoxides in the solution phase (such as pure hydrazine and hydrazine hydrate) may involve other important elementary steps that are not shown in the gas-phase reaction reported herein, which warrants further investigation. Nonetheless, the improved understanding of the hydrazine-epoxide interaction will assist in better understanding atomistic mechanisms underlying the hydrazine reduction of GO sheets.

ACKNOWLEDGMENTS

One of the authors (G.S.H.) greatly acknowledges the Welch Foundation for financial support. Another author (M.C.K.) acknowledges SBS Foundation of Seoul for financial support for his sabbatical leave. All our calculations were performed using supercomputers in Texas Advanced Computing Center at the University of Texas at Austin.

[1] K. S. Novoselov, A. K. Geim, S. V. Morozov, D. Jiang, Y. Zhang, S. V. Dubonos, I. V. Grigorieva, and A. A. Firsov, Science **306**, 666 (2004).
[2] K. S. Novoselov, A. K. Geim, S. V. Morozov, D. Jiang, M. I. Katsnelson, I. V. Grigorieva, S. V. Dubonos, and A. A. Firsov, Nature (London) **438**, 197 (2005).
[3] K. S. Novoselov, D. Jiang, F. Schedin, T. J. Booth, V. V. Khotkevich, S. V. Morozov, and A. K. Geim, Proc. Natl. Acad. Sci. U.S.A. **102**, 10451 (2005).
[4] C. Gómez –Navarro, R. T. Weitz, A. M. Bittner, M. Scolari, A. Mews, M. Burghard, and K. Kern, Nano Lett. **7**, 3499 (2007).
[5] N. A. Kotov, Nature (London) **442**, 254 (2006).
[6] S. Stankovich, D. A. Dikin, G. H. B. Dommett, K. M. Kohlhaas, E. J. Zimney, E. A. Stach, R. D. Piner, S. T. Nguyen, and R. S. Ruoff, Nature (London) **442**, 282 (2006).
[7] D. A. Dikin, S. Stankovich, E. J. Zimney, R. D. Piner, G. H. B. Dommett, G. Evmenenkos, S. T. Nguyen, and R. S. Ruoff, Nature (London) **448**, 457 (2007).
[8] S. Stankovich, R. D. Piner, X. Chen, N. Wu, S. T. Nguyen, and R. B. Ruoff, J. Mater. Chem. **16**, 155 (2006).
[9] S. Stankovich, R. D. Piner, S. T. Nguyen, and R. B. Ruoff, Carbon **44**, 3342 (2006).
[10] S. Stankovich, D. A. Dikin, R. D. Piner, K. A. Kohlhaas, A. Kleinhammes, Y. Jia, Y. Wu, S. T. Nguyen, and R. B. Ruoff, Carbon **45**, 1558 (2007).

[11] V. C. Tung, M. J. Allen, Y. Yang, and R. B. Kaner, Nat. Nanotechnol. **4**, 25 (2009).
[12] J. P. Perdew and Y. Wang, Phys. Rev. B **45**, 13244 (1992).
[13] G. Kresse and J. Furthmuller, VASP the guide, Vienna University of Technology, 2001.
[14] D. C. Sorescu, K. D. Jordan, and P. Avouris, J. Phys. Chem. B **105**, 11227 (2001).
[15] A. Incze, A. Pasturel, and C. Chatillon, Surf. Sci. **537**, 55 (2003).
[16] A. Jelea, F. Marinelli, Y. Ferro, A. Allouche, and C. Brosset, Carbon **42**, 3189 (2004).
[17] J.-L. Li, K. N. Kudin, M. J. McAllister, R. K. Pru'homme, I. A. Aksay, and R. Car, Phys. Rev. Lett. **96**, 176101 (2006).